Kinetics and Catalysis, Vol. 41, No. 1, 2000, pp. 61–70. Translated from Kinetika i Kataliz, Vol. 41, No. 1, 2000, pp. 71–81.

Catalytic Decomposition of Azomethane and Reactions of Adsorbed Methyl Radicals on the Molybdenum Surface

M. Yu. Kislyuk, I. I. Tret'yakov†, V. V. Savkin, and M. Yu. Sinev

Semenov Institute of Chemical Physics, Russian Academy of Sciences, Moscow, 117977 Russia

Received April 24, 1998

Abstract—The methods of temperature-programmed reaction/desorption (TPR/TPD) are used to study azomethane ($CH_3N{=}NCH_3$) decomposition and the reactions of the products of its pyrolysis ($CH_3^{\bullet}$ radicals and N_2) on the polycrystalline molybdenum surface. A TPR spectrum of adsorbed azomethane decomposition shows mainly N_2, H_2, and unreacted azomethane. Upon preliminary adsorption of azomethane pyrolysis products on a catalyst sample, a TPR spectrum shows N_2, H_2, and CH_4 in comparable amounts. The difference in the composition of desorption products found for these two types of experiments shows that, in the decomposition of adsorbed azomethane, surface methyl moieties are not formed. The rate constants were calculated for the dissociation of adsorbed CH_3, CH_2, and CH, recombination of hydrogen atoms with each other and with CH_3 and CH_2, and the recombinative desorption of nitrogen atoms.

INTRODUCTION

Recently, experimental evidence has been found for the occurrence of many reactions of oxidative catalysis via the formation and a successive transformations of free radicals [1–3]. Secondary reactions of radicals resulting in the formation of final products may occur both in the gas phase and on the surface after their trapping back by the surface. The overall rate of the process and the composition of the reaction mixture are determined by many reactions of radicals and the products of their adsorption on the active sites of a catalyst. Therefore, the study of free radical trapping by various surfaces and their transformations on these surfaces is of great interest.

In a number of processes for the catalytic conversion of methane, a primary species formed by hydrocarbon activation is methyl radical [4, 5]. The overall rate of the process and the selectivities to various products depend on both the kinetics of methyl radical reactions on the surface and on the stoichiometry of reactions between species formed from methyl radical adsorption. Specifically, it has been shown [6] that in the presence of a binary catalyst consisting of an oxide capable of generating methyl radicals and a metal, which is itself inactive, the overall rate of methane conversion increases nonadditively and the composition of products formed in the reaction drastically changes. This is due to the secondary reactions of methyl radicals on the metal surface.

These data show that the study of methyl radical adsorption and its secondary reactions on the surface is of substantial interest. The following clean and oxidized surfaces were examined by this time: Pt(111) [7], Ni(100) and Ni(111) [8, 9], and oxidized Mo(100) [10].

The thermal decomposition of azomethane is often used as a method for generating methyl radicals [7, 10]. The catalytic decomposition of azomethane has only been studied in detail on platinum [11] and rhodium [12], and a number of products were found: H_2, HCN, CH_3NH_2, and C_2N_2. In addition to these products, the rhodium surface also generated dinitrogen.

In this work, we studied the catalytic decomposition of azomethane and reactions of $CH_3^{\bullet}$ radicals on the surface of polycrystalline molybdenum. This surface is interesting because it forms strong chemisorptive bonds and dissociatively chemisorbs many molecules, including dinitrogen. The temperature-programmed reaction/desorption (TPR/TPD) method coupled with mass spectrometry enabled the determination of the composition of products desorbing from the surface and kinetic measurements [13].

EXPERIMENTAL

Experiments were carried out in an ultrahigh vacuum (UHV) setup with a ceiling for residual gases of 5×10^{-10} torr. Figure 1 shows the schematic of a vacuum chamber.

A sample made of molybdenum (99.99%) foil ($10 \times 4 \times 0.05$ mm) was placed in the middle of the vacuum chamber on a manipulator that enabled sample rotation by 360° and the exposure of its front face either to the molecular beam of gas or to the mass spectrometer inlet. The temperature of a sample heated with electric current was measured with a W–Re thermocouple welded to the backside of the sample. Before experiments, the sample was cleaned from gases and carbon

† Deceased.

0023-1584/00/4101-0061$25.00 © 2000 MAIK "Nauka/Interperiodica"

impurities by prolonged heating in an oxygen atmosphere ($P = 10^{-7}$ torr) at $T = 1800$ K. This procedure was repeated before each experimental series.

Azomethane, the products of its pyrolysis (N_2 and $CH_3^{\bullet}$), and other gases were supplied by an effusion molecular beam and adsorbed on the sample front, which was kept at room temperature. The molecular beam was generated by a quartz capillary. The sample temperature (~25°C) was kept constant.

According to the published data [10], during azomethane pyrolysis in the mixture with argon under the optimal beam conditions, the portion of methyl radicals in the products was 14%. The molecular beam also contained Ar (47%), N_2 (18%), CH_4 (13%), C_2H_6 (5%), H_2 (2%), and CH_3NNCH_3 (0.4%). Unlike the conditions for molecular beam formation used in [10], in our experiments, starting azomethane contained no inert gas (argon). Under UHV conditions, this may lead to a decrease in the concentration of ethane, which is a product of termolecular methyl radical recombination, in pyrolysis products.

Upon the admission of gases, the temperature was increased according to a program from room temperature to 1500 K. The rate of product desorption was registered using an omegatron mass spectrometer. After 10–20-min exposure, the results of desorption measurements stopped changing; therefore, we assumed that this time is sufficient for reaching monolayer saturation. The rates of heating were varied between 30 and 300 K/s.

RESULTS AND DISCUSSION

Catalytic Decomposition of Azomethane

Figure 2 shows the TPR spectrum of azomethane decomposition registered after molybdenum surface saturation with this substance. This figure shows that nitrogen and hydrogen are the major products desorbing from the surface. Some amount of unreacted azomethane was also observed in desorption products. The temperatures of maxima (T_{max}) of the corresponding peaks were 1200, 710, and 680 K.

Because other nitrogen-containing products of azomethane decomposition are absent from the TPR spectra, we suggest that adsorbed nitrogen atoms recombine only with each other. They do not react with azomethane or with the products of its decomposition. This is contrasting to the data on azomethane decomposition over platinum [11] reported by Jentz *et al.*, who observed a number of gaseous nitrogen-containing products (CH_3NH_2, HCN, and C_2N_2) and did not observe molecular nitrogen. On the molybdenum surface, which is characterized by higher binding energies of H, C, and N atoms than platinum, virtually complete azomethane dissociation into elements probably occurs already at low temperatures. On further heating, hydrogen and then nitrogen desorb from the surface.

Virtually complete absence of carbon in desorption products in this series of runs is probably due to its dissolution in the bulk of a sample at high temperatures. This is evident from the fact that the TPR spectra (Fig. 2) are reproducible in a series of several tens of runs despite the formation of carbon in a monolayer (ML) amount in each run. If the coverage of the molybdenum surface by carbon atoms was high or surface carbide was formed, the adsorption properties of a sample would progressively change, and this would affect the dissociative adsorption of nitrogen. However, this was not the case in our experiments.

We registered TPD spectra of nitrogen and hydrogen after their separate adsorption on the sample surface. These spectra were identical to those observed in the temperature-programmed decomposition of

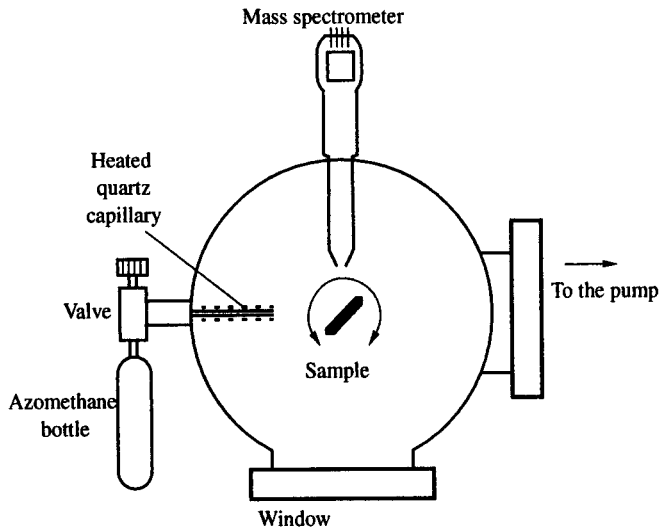

Fig. 1. Schematic of the vacuum chamber.

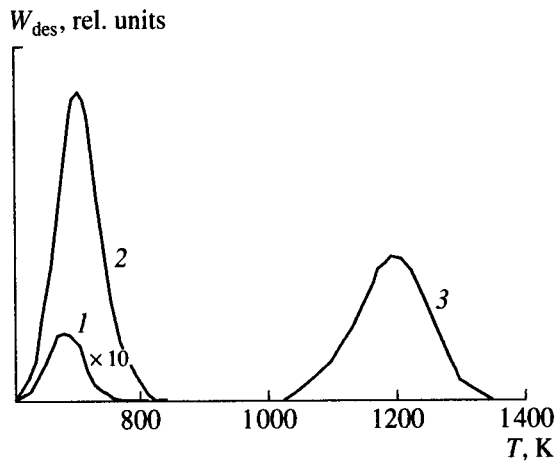

Fig. 2. TPR spectrum of the catalytic azomethane decomposition registered after its monolayer adsorption on the polycrystalline molybdenum surface: (*1*) azomethane; (*2*) hydrogen; and (*3*) nitrogen. The rate of heating for *1* and *2* is 300 K/s; the rate of heating for *3* is 130 K/s.

adsorbed azomethane. Strong dissociative adsorption of nitrogen on the sample points to the fact that the surface largely consists of clean molybdenum and is not covered with carbon or molybdenum carbide. Probably, we dealt with the steady-state condition of the sample, whose surface is cleaned from carbon during heating because of carbon dissolution in the metal bulk. The data also suggest that the rate of hydrogen-atom recombination is independent of the surface in the presence of nitrogen atoms. We used these conclusions in further kinetic analysis of the processes in the adsorbed layer formed by azomethane pyrolysis products.

The activation energies E and preexponential factors k^0 of azomethane, nitrogen, and hydrogen desorption were calculated by the formulas [14]

$$\ln(F/\ln F) = [rT_1T_2\ln(\theta_1/\theta_2)]/[T_{max}(T_2 - T_1)], \quad (1)$$

$$E = RT_{max}\ln(F/\ln F), \quad (2)$$

where $F = (k^0\theta_{max}^{r-1}T_{max})/b$; T_1 and T_2 are the temperatures for the half-maximum rate of desorption; θ_{max}, θ_1, and θ_2 are surface coverages at T_{max}, T_1, and T_2, respectively; r is the kinetic order of desorption and b is the rate of heating, which was 130–300 K/s in the catalytic decomposition of azomethane.

The $\ln(\theta_1/\theta_2)$ values for the first- and second-order desorption were determined earlier [14]: 2.3 and 1.6, respectively.

The peaks of nitrogen and hydrogen in the TPR spectrum were analyzed using the second-order rate law, and that for azomethane was analyzed with the first-order rate law. Because surface coverages were used instead of concentrations, all rate constants are in reciprocal seconds. The rate constants estimated for desorption are as follows:

	H_2	N_2	$CH_3N{=}NCH_3$
E, kJ/mol	160 ± 10	270 ± 15	130 ± 20
$\log k^0$, [s^{-1}]	13.6 ± 1.0	12.5 ± 1.5	10.6 ± 2.0

These parameters of desorption rate constants for hydrogen and nitrogen agree with the literature data [15–18], which confirms that these gases are in dissociated form on the molybdenum surface.

The experimental data suggest that azomethane almost completely decomposes on the molybdenum surface in the TPR regime, and the rate of its decomposition does not limit nitrogen or hydrogen desorption.

Therefore, the catalytic decomposition of adsorbed azomethane on molybdenum can be described by the following reactions:

$$\begin{aligned}
&1)\ [CH_3N{=}NCH_3] \longrightarrow CH_3N{=}NCH_3\\
&2)\ [CH_3N{=}NCH_3] \rightleftharpoons 2[NCH_3]\\
&3)\ [NCH_3] \rightleftharpoons [NCH_2] + [H]\\
&4)\ [NCH_2] \longrightarrow [C] + [N] + 2[H] \qquad (I)\\
&5)\ 2[H] \longrightarrow H_2\\
&6)\ 2[N] \longrightarrow N_2\\
&7)\ [C] \longrightarrow \{C\}.
\end{aligned}$$

In these reactions, gaseous products are without brackets, surface species are in square brackets, and carbon dissolved in the metal bulk is in braces.

Step 3 in scheme (I) is reversible based on the following estimates. The energy of the C–H bond in azomethane is close to the C–H bond in hydrocarbons (i.e., 400–420 kJ/mol). The energy of hydrogen atom binding to the surface q can be estimated from the energy of hydrogen molecule dissociation by the equation

$$q = (E + D)/2, \quad (3)$$

assuming that the dissociative adsorption of hydrogen on molybdenum occurs with zero activation energy; that is, E is equal to adsorption heat. Upon substituting the values of E and D into equation (3), we have q = 285 ± 20 kJ/mol. That is, forward step 3 is endothermic, and this suggests that it may occur in the backward direction.

It is likely that, after the abstraction of the first hydrogen atom from the NCH_3 group, the remaining group becomes unstable and rapidly dissociates into elements. This is shown as step 4. The TPR spectra do not show even trace amounts of CH_4, C_2H_6, C_2H_4, or C_2H_2, which can be formed via the recombination of intermediate species; therefore, step 4 should be fast.

Reactions of N and CH_3^* in the Mixed Adsorbed Layer

In the study of the adsorption and reactions of azomethane pyrolysis products, it was necessary to determine the optimal temperatures for azomethane thermal decomposition. For this purpose, we registered the mass spectra of the gas phase during the uninterrupted supply of azomethane through the quartz capillary heated to various temperatures. The pressure in the vacuum chamber was kept at the level of 5×10^{-8} torr. Figure 3 shows these mass spectra. As can be seen, at 300–800 K, the mass spectrum remains unchanged and corresponds to pure azomethane with traces of residual gases. At higher temperatures (>800 K), the partial pressure of azomethane decreases as evident from the lowered peaks with m/e = 58 (the molecular ion) and m/e = 43 (the $N{=}NCH_3^+$ ion) and other characteristic peaks. Finally, at temperatures of the quartz capillary above 1070 K, azomethane is absent from the gas phase.

In further experiments, azomethane pyrolysis was carried out at a quartz capillary temperature of 1100 K. As noted above, in addition to methyl radicals and nitrogen molecules, the beam of pyrolysis products contained methane, ethane, and molecular hydrogen. In special experiments under analogous conditions (the

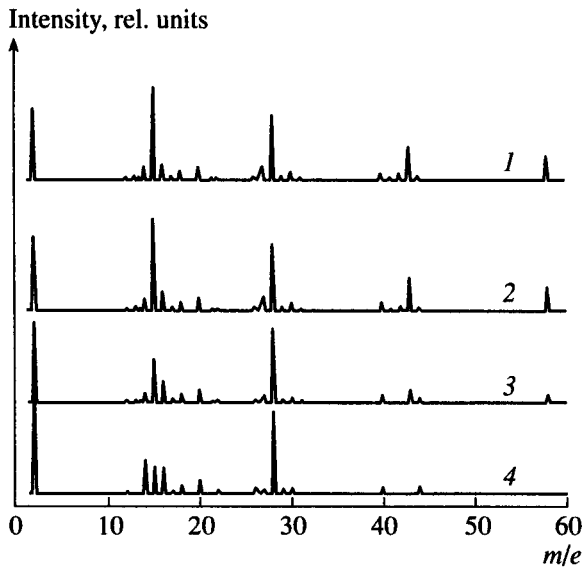

Fig. 3. Mass spectra of the gas phase registered during the uninterrupted supply of azomethane into the vacuum chamber through the quartz capillary heated to (*1*) 300, (*2*) 800, (*3*) 900, and (*4*) 1100 K.

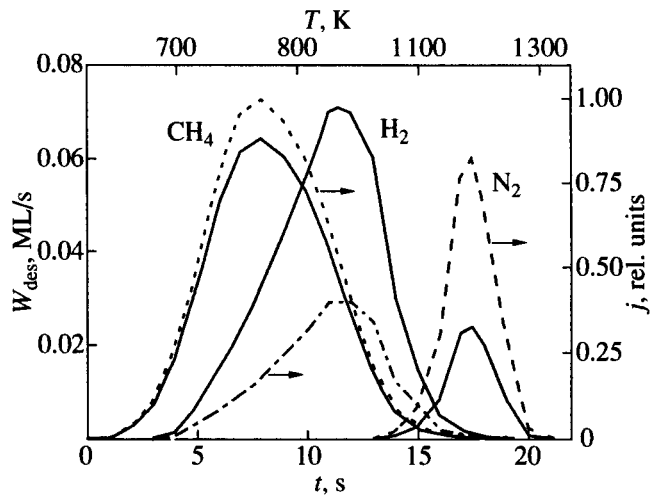

Fig. 4. TPR spectrum observed after monolayer adsorption of the azomethane pyrolysis products (N_2 and CH_3^*) on the molybdenum surface. Dashed lines show the ionic currents j corresponding to H_2^+, N_2^+, and CH_4^+. Ordinary lines show the absolute rates of desorption calculated using equations (6)–(9).

room temperature and exposure for up to 20 min), we showed that methane and ethane are not adsorbed on the molybdenum surface. A possible effect of hydrogen, which is present in the beam, will be discussed below.

Figure 4 shows a typical TPR spectrum observed upon the adsorption of azomethane pyrolysis products at their surface coverage close to saturation, which we assumed to be 1 ML. The rate b of sample heating was 37 K/s in these experiments. As can be seen from the figure, nitrogen, hydrogen, and methane desorb from the surface in comparable amounts. The values of T_{max} for these gases are 1200, 1000, and 870 K, respectively. The dashed lines show the experimental plots of ionic currents j in relative units versus time and the ordinary lines show the plots for the absolute desorption rates of the corresponding gases (W, ML/s); their calculation is explained below.

Note that the peak of nitrogen is observed at the same temperature as in the experiments on the catalytic decomposition of azomethane and virtually coincides with the TPD spectra recorded after N_2 adsorption on the molybdenum surface. The calculation of the rate parameters for nitrogen desorption according to equations (1) and (2) gives us $E = 280 \pm 15$ kJ/mol, $\log k^0 = 13.5 \pm 1.5$, which agrees with the above results within the experimental accuracy.

The TPR spectrum of hydrogen registered under these conditions differs from TPR/TPD spectra observed after molecular hydrogen adsorption and in the catalytic decomposition of azomethane on molybdenum. The difference is in the form of a peak (elongated front) and in T_{max}.

Comparison of the results obtained in the above two types of experiments uncovers their fundamental difference. Specifically, when azomethane decomposes on molybdenum, methane is not formed. In the TPR in the mixed adsorbed layer of N and CH_3^*, methane is formed in substantial amounts. This fact indicates different compositions of adsorbed layers and the absence of methyl groups from the surface in the case of azomethane decomposition. This means that the catalytic decomposition of azomethane on the molybdenum surface does not occur via the primary scission of the N–CH_3 bond.

The absence of nitrogen-containing compounds other than N_2 from the TPR spectra suggests that adsorbed nitrogen atoms recombine only with each other and do not react with methyl radicals or the products of methyl decomposition.

The reactions in the mixed adsorbed layer over molybdenum containing N and CH_3^* may be described by the following scheme:

$$\begin{aligned}
&(1)\ [CH_3] \rightleftharpoons [CH_2] + [H],\\
&(2)\ [CH_2] \rightleftharpoons [CH] + [H],\\
&(3)\ [CH] \rightleftharpoons [C] + [H],\\
&(4)\ 2[N] \longrightarrow N_2,\\
&(5)\ 2[H] \longrightarrow H_2,\\
&(6)\ [CH_3] + [H] \longrightarrow CH_4,\\
&(7)\ [C] \longrightarrow \{C\}.
\end{aligned} \qquad \text{(II)}$$

In this scheme, the notation for the species is the same as in scheme (I). Steps 1–3 are considered reversible for the same reason as before.

Notably, in the process under study, adsorbed methyl radicals recombine only with adsorbed hydrogen atoms but not with each other. Two carbon atoms from methyl groups probably cannot close over each other because of steric hindrances, whereas small and mobile hydrogen atoms may approach a carbon atom on the surface or attack it from the metal bulk because hydrogen is highly soluble in metals [19].

Dinitrogen desorbs from the surface when all other adsorbates except carbon already left the surface. Thus, the effect of adsorbed nitrogen on the reactions of adsorbed methyl radicals and products of its decomposition on the molybdenum surface consists mainly in blocking surface sites.

The TPR spectra of hydrogen and methane (Fig. 4) cannot be processed with equations (1) and (2) because H_2 and CH_4 are the products from a multistep process rather than desorption. For the quantitative analysis of these spectra, we used scheme (II).

TPR spectra shown as plots of ionic currents corresponding to the molecular ions H_2^+, CH_4^+, and N_2^+ (m/e = 2, 16, and 28) versus time and temperature (Fig. 4) provide only a qualitative picture for the molecules desorbing to the gas phase.

For the quantitative analysis, it was necessary to recalculate the apparent values of ionic currents into the absolute rates of gaseous product formation. According to [20], the current j corresponding to any specific ion is proportional to the partial pressure P of the gas:

$$j \sim \alpha\beta P, \tag{4}$$

where α is the ionization cross-section of a molecule, and β is the portion of ion in the mass spectrum of a substance.

The ratio of ionization cross-sections of hydrogen, methane, and nitrogen is 1 : 2.5 : 2.5 [19], and the values of β measured for the molecular ions are 0.98, 0.5, and 0.9, respectively.

The partial pressure of gas desorbing in the vacuum system and its evacuation are described by the equation [20]

$$V(dP/dt) = W_{des} - SP, \tag{5}$$

where V is the volume of the vacuum chamber, t is time, W_{des} is the desorption rate, and S is the evacuation rate.

Under our experimental conditions, the values of S measured for hydrogen, methane, and nitrogen are 100, 50, and 40 l/s, respectively. At these high rates of evacuation, the left-hand side of equation (5) can be equalized to zero. Then, equations (4) and (5) lead to a simple relation between the rate of desorption of any specific gas and the corresponding ionic current:

$$W_{des} \sim (jS)/(\alpha\beta). \tag{6}$$

This formula enables the calculation of the relative values of gas desorption rates. The absolute values of W (ML/s) for H_2, CH_4, and N_2 (W_{H_2}, W_{CH_4}, and W_{N_2}) were obtained from the material balance equation

$$\theta^0_{CH_3} + \theta^0_N = 1, \tag{7}$$

which involves the initial surface coverages by methyl radicals $\theta^0_{CH_3}$ and nitrogen atoms θ^0_N. Note that this equation does not take into account the initial surface coverage by hydrogen θ^0_H, although hydrogen is present in the molecular beam of azomethane pyrolysis products according to the data reported by Smudde *et al.* [10]. We will show below that our experimental data suggest that the initial surface coverage of the molybdenum surface by hydrogen is negligible.

The values of $\theta^0_{CH_3}$ and θ^0_N can be described in the following form:

$$\theta^0_{CH_3} = \left(4\int_0^\infty W_{CH_4}dt + 2\int_0^\infty W_{H_2}dt\right)/3, \tag{8}$$

$$\theta^0_N = 2\int_0^\infty W_{N_2}dt. \tag{9}$$

The TPR spectra shown with dashed lines in Fig. 4 were calculated using equations (6)–(9) to obtain the absolute desorption rates (ML/s) for the gases (ordinary lines). Thus, the TPR spectra were normalized to determine the following initial coverages: $\theta^0_{CH_3}$ = 0.87 and θ^0_N = 0.13.

In further analysis, we will use the following notation system: θ_H, θ_N, θ_{CH_3}, θ_{CH_2}, θ_{CH}, and θ are the current surface coverages with H, N, CH_3, CH_2, CH, and the portion of clean surface, respectively; θ_C is the overall amount of carbon on the surface and in the bulk formed during one experiment; and k_i and k_{-i} are the rate constants for the ith step in scheme (II) in the forward and backward directions.

We processed the TPR spectra (Fig. 4) by first determining the $\theta_H(t)$ dependence assuming that the rate of hydrogen desorption is independent of the presence of nitrogen atoms on the surface. We also considered that the rate of hydrogen desorption is independent of the presence of other species on the surface. Therefore, the following rate law can be used that describes hydrogen desorption

$$W_{H_2} = k_5(\theta_H)^2. \tag{10}$$

The apparent dependence $W_{H_2}(t)$ and the rate constant $k_5 = 4 \times 10^{13}\exp(-160/RT)$ s^{-1} measured in the experiments with preliminary H_2 adsorption were substituted into this equation. Henceforth, the activation energies are in kJ/mol. Figure 5 shows the dependence $\theta_H(t)$ thus

obtained. As can be seen, the θ_H can be neglected not only at the initial moment, but also up to 650 K.

This result should be discussed in more detail.

As mentioned above, the molecular beam of azomethane pyrolysis products should contain noticeable amounts of molecular hydrogen, which can dissociatively adsorb on the molybdenum surface under the conditions of our experiments. If atomic hydrogen were present on the surface from the start (that is, after adsorption at room temperature), then a noticeable rate of its recombinative desorption would be observed at 600 K, but this was disconfirmed in experiments. This fact can be explained by hydrogen recombination with gas-phase methyl radicals that competes with adsorption:

$$[H] + CH_3^{\cdot} \longrightarrow CH_4.$$

This reaction efficiently removes adsorbed hydrogen from the surface.

Because carbon desorbs from the surface only in the form of methane, the material balance condition with respect to carbon provides us with the expression for the overall surface coverage with carbon-containing species ($\theta_\Sigma = \theta_{CH_3} + \theta_{CH_2} + \theta_{CH} + \theta_C$):

$$\theta_\Sigma(t) = \theta^0_{CH_3} - \int_0^t W_{CH_4} dt. \quad (11)$$

The current value $\theta_N(t)$ was determined from the equation,

$$\theta_N(t) = 2\int_t^\infty W_{N_2} dt, \quad (12)$$

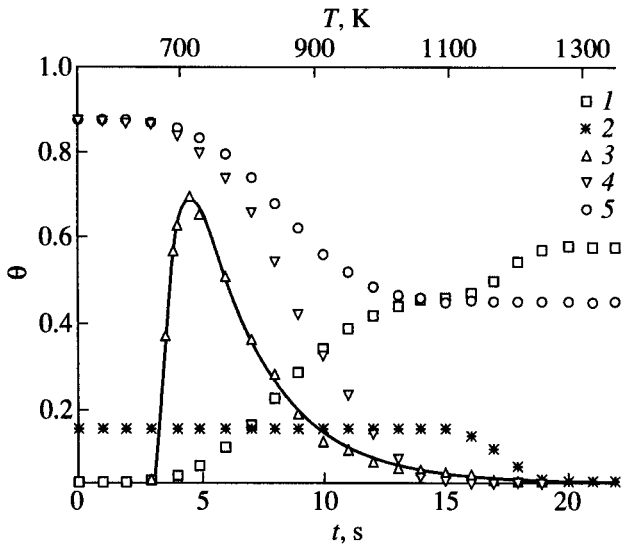

Fig. 5. Dependences of (*1*) θ, (*2*) θ_N, (*3*) $\theta_H \times 100$, (*4*) θ_{CH_3}, and (*5*) $\theta_\Sigma = \theta_{CH_3} + \theta_{CH_2} + \theta_{CH} + \theta_C$ on time (temperature) calculated by equations (10)–(13), (19). The ordinary lines refer to 100 θ_H calculated by equation (27).

and $\theta(t)$ can be found from the balance of surface concentrations

$$\theta(t) = 1 - \theta_N - \theta_H - \theta_\Sigma. \quad (13)$$

Figure 5 shows the plots of θ, θ_N, θ_H, and θ_Σ versus time (temperature).

The next task was to determine current surface coverages by methyl groups and other carbon-containing species.

Obviously, the coverage with methyl θ_{CH_3} initially (at low temperatures) is the highest and the values of θ_{CH_2}, θ_{CH}, and θ_C are relatively small. According to scheme (II), CH_2, CH, and C are formed by successive steps of hydrogen abstraction. Therefore, the following inequality should be fulfilled:

$$\theta_{CH_2} > \theta_{CH} > \theta_C. \quad (14)$$

To a first approximation, we assumed for the initial period that

$$\theta_\Sigma = \theta_{CH_3} + \theta_{CH_2}. \quad (15)$$

The equation of material balance with respect to hydrogen during this period is

$$3\theta_{CH_3} + 2\theta_{CH_2} = 3\theta^0_{CH_3} - 4\int_0^t W_{CH_4} dt - 2\int_0^t W_{H_2} dt - \theta_H. \quad (16)$$

With equations (11), (15) and (16), we arrive at

$$\theta_{CH_2} = \int_0^t W_{CH_4} dt + 2\int_0^t W_{H_2} dt + \theta_H, \quad (17)$$

$$\theta_{CH_3} = \theta^0_{CH_3} - 2\int_0^t W_{CH_4} dt - 2\int_0^t W_{H_2} dt - \theta_H. \quad (18)$$

Then, using the equation

$$W_{CH_4} = k_6 \theta_H \theta_{CH_3}, \quad (19)$$

we determined the rate constant k_6 for the recombination of hydrogen atoms with methyl groups, which is adequately described by the Arrhenius equation (see Fig. 6) in this temperature range

$$k_6 = 1.3 \times 10^{9\pm1} \exp((-117 \pm 6)/RT)\ s^{-1}. \quad (20)$$

We assumed further that equation (20) correctly describes k_6 over the whole range of temperatures and calculated the dependence of θ_{CH_3} on time (temperature) using equation (19) (see Fig. 5).

The sum $\theta_{CH_2} + \theta_{CH} + \theta_C$ can be determined by subtracting θ_{CH_3} from the overall surface coverage by carbon-containing species.

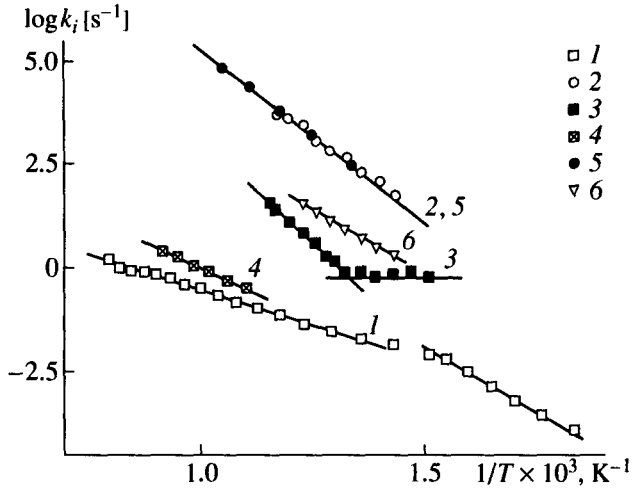

Fig. 6. Temperature dependences of the rate constants obtained from analysis of TPR spectra (Fig. 4) using scheme (II): (*1*) k_1, (*2*) k_{-1}, (*3*) $k_2 + k_2^*$, (*4*) $k_{3\text{eff}}$, (*5*) k_5, and (*6*) k_6.

Then, we applied the material balance with respect to hydrogen to the whole range of temperatures while neglecting θ_{CH}:

$$3\theta_{CH_3} + 2\theta_{CH_2} + \theta_{CH} = 3\theta^0_{CH_3} - 4\int_0^t W_{CH_4}dt - 2\int_0^t W_{H_2}dt - \theta_H. \quad (21)$$

Because θ_{CH_3} was determined earlier, this equation enabled us to determine the sum $2\theta_{CH_2} + \theta_{CH}$ as a function of time (temperature) shown in Fig. 7. This dependence has the form of two overlapping peaks.

If scheme (II) is considered true, then the adsorbed species CH_2 and CH are intermediate products in the successive steps of hydrogen abstraction. Therefore, the first, low-temperature peak should correspond to θ_{CH_2}, and the other peak should correspond to θ_{CH}. Upon determining θ_{CH_3}, θ_{CH_2}, and θ_{CH}, we calculated θ_C using the equation

$$\theta_C = \theta_\Sigma - \theta_{CH_3} - \theta_{CH_2} + \theta_{CH}. \quad (22)$$

Thus, we obtained the time (temperature) dependences for all coverages by carbon-containing species. They are shown in Figs. 7 and 8.

Note that carbon starts accumulating on the surface when the concentration of CH groups is still undetectable. The $\theta_C(t)$ dependence suggests that the rate of carbon formation drastically increases with the appearance of CH groups.

The results of this calculation suggest that, in addition to the reactions described by the simplest scheme (II), one should take into account the process of carbon formation directly from CH_2 groups:

$$(2^*)\ [CH_2] \longrightarrow [C] + 2[H],$$

with the rate constant k_2^*.

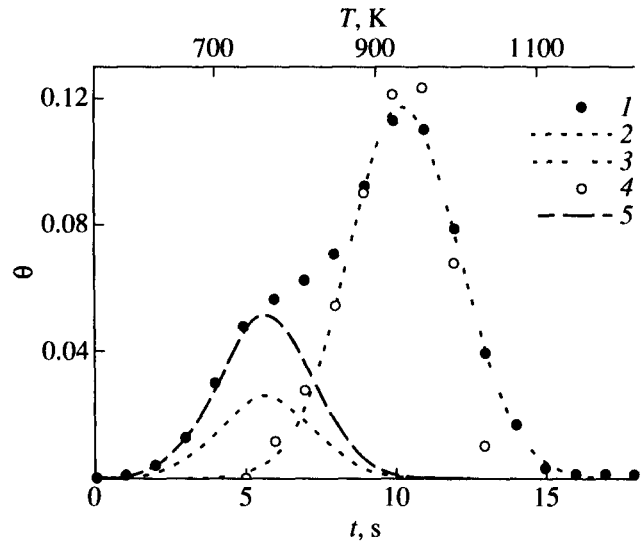

Fig. 7. Dependence of $2\theta_{CH_2} + \theta_{CH}$ on time (temperature) (*1*) calculated by equation (21) and its decomposition into (*2*) θ_{CH_2} and (*3*) θ_{CH} calculated by equations (29) and (30), respectively; (*4*) θ_{CH} calculated by equation (25) neglecting the reverse reaction; (*5*) $2\theta_{CH_2}$.

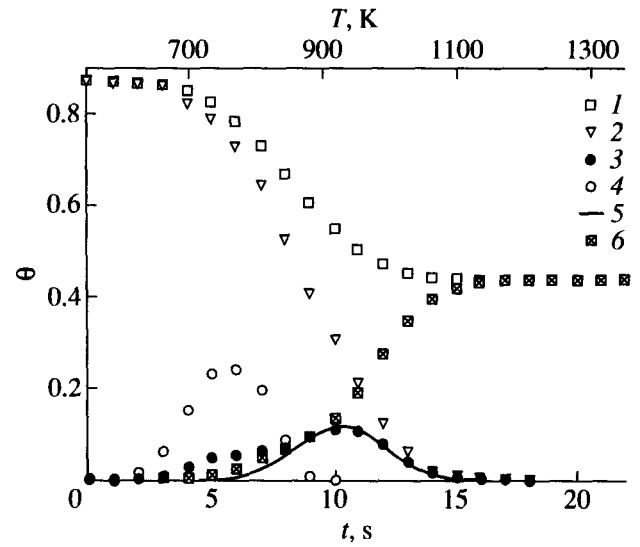

Fig. 8. The dependences of surface concentrations of carbon-containing species on time (temperature), calculated from the TPR spectra (Fig. 4) by equations (11), (19)–(22): (*1*) θ_Σ, (*2*) θ_{CH_3}, (*3*) $2\theta_{CH_2} + \theta_{CH}$, (*4*) $10\theta_{CH_2}$, (*5*) θ_{CH}, and (*6*) θ_C.

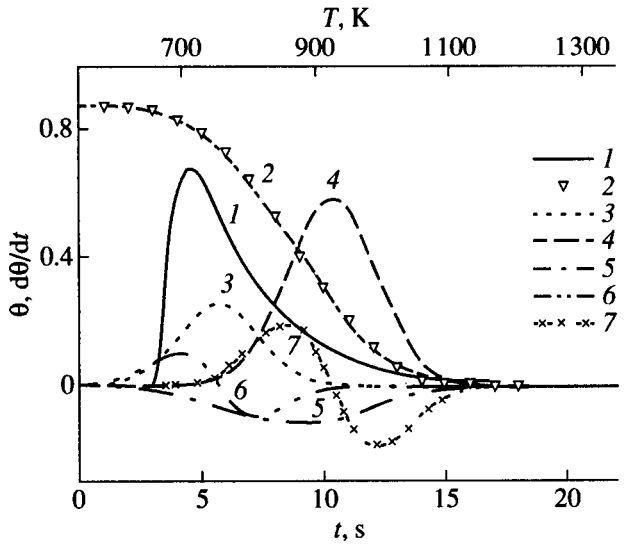

Fig. 9. Plots of analytical functions and their derivatives that describe the dependences of surface concentrations of carbon-containing species on time (temperature): (*1*) $100\,\theta_H$; (*2*) θ_{CH_3}; (*3*) $10\theta_{CH_2}$; (*4*) $5\theta_{CH}$, (*5*) $d\theta_{CH_3}/dt$, (*6*) $10d\theta_{CH_2}/dt$, and (*7*) $5d\theta_{CH}/dt$.

Then, the rate laws for all carbon-containing species on the surface are

$$-d\theta_{CH_3}/dt = k_1\theta_{CH_3} + W_{CH_4} - k_{-1}\theta_{CH_2}\theta_H, \quad (23)$$

$$d\theta_{CH_2}/dt = k_1\theta_{CH_3} - k_{-1}\theta_{CH_2}\theta_H - (k_2 + k_2^*)\theta_{CH_2} + k_{-2}\theta_{CH}\theta_H, \quad (24)$$

$$d\theta_{CH}/dt = k_2\theta_{CH_2} - k_{-2}\theta_{CH}\theta_H - k_3\theta_{CH} + k_{-3}\theta_C\theta_H, \quad (25)$$

$$d\theta_C/dt = k_2^*\theta_{CH_2} + k_3\theta_{CH} - k_{-3}\theta_C\theta_H. \quad (26)$$

To calculate the rates of the formation and consumption of surface species, we approximated the dependences $\theta_H(t)$, $\theta_{CH_3}(t)$, $\theta_{CH_2}(t)$, and $\theta_{CH}(t)$ by the continuously differentiable analytical functions

$$\theta_H = 11.36[(t-3)^{3.24}]\exp\{-7.524[(t-3)^{0.37}]\}, \quad (27)$$

$$\theta_{CH_3} = 0.87\exp[-(t/9.847)^{3.448}], \quad (28)$$

$$\theta_{CH_2} = 0.0255\exp\{-[(t-5.672)/2.245]^2\}, \quad (29)$$

$$\theta_{CH} = 0.1168\exp\{-[(t-10.32)/2.623]^2\}, \quad (30)$$

as shown in Fig. 9. This figure also shows the derivatives of surface concentrations obtained by the differentiation of approximating functions. Figures 5, 7, and 9 illustrate high accuracy in the approximation of the surface concentrations by these functions (the plots of functions (27)–(30) are shown together with points that describe experimental values.

Then, equation (23) can be used to determine the rate constant k_1 if we neglect the term $k_{-1}\theta_{CH_2}\theta_H$. Figure 6 shows the Arrhenius plot for this rate constant. A characteristic salient point at $T \approx 650$–700 K catches the eye. At lower temperatures, the rate constant is described by the equation

$$k_1 = 1.1 \times 10^{7\pm1}\exp((-116 \pm 4)/RT)\ s^{-1}, \quad (31)$$

and at higher temperatures, the rate constant is described by the equation

$$k_1 = 7.4 \times 10^{2\pm0.5}\exp((-64 \pm 2)/RT)\ s^{-1}. \quad (32)$$

The salient point on the Arrhenius plot suggests that the rate of the reverse process (the recombination of the CH_2 group with H) can be neglected in equation (23) only at low temperatures. Incidentally, according to our estimates (see Fig. 7), at 650–700 K, the CH_2 groups appear on the surface in noticeable concentrations.

Then, we assumed that equation (31) describes the rate constant k_1 in the whole temperature range and substituted equation (31) into (23). The rate constant k_{-1} thus obtained (Fig. 6) is

$$k_{-1} = 1.1 \times 10^{13\pm1}\exp((-151 \pm 4)/RT). \quad (33)$$

The sum of the rate constants $k_2 + k_2^*$ was determined as a difference between equations (23) and (24) by neglecting the term $k_{-2}\theta_{CH}\theta_H$:

$$k_2 + k_2^* = -d\theta_{CH_3}/dt - d\theta_{CH_2}/dt - W_{CH_4}/\theta_{CH_2}. \quad (34)$$

The dependence of the sum of the rate constants on temperature is shown in Figs. 6 and 10.

A characteristic inflection point seen in Fig. 6 suggested that this dependence can be described by the sum of Arrhenius functions as shown in Fig. 10.

The first of these functions characterized by a small preexponential factor and an activation energy close to zero can be assigned to k_2^* because this constant contributes mainly to the sum at low temperatures. This allows us to explain the formation of surface carbon with CH formation.

The second function describes the constant k_2, which is characterized by a normal preexponential factor and a high activation energy:

$$k_2 = 2 \times 10^{14\pm2}\exp((-210 \pm 10)/RT). \quad (35)$$

The rate constant k_3 was determined from equation (26) in the region of high temperatures when the term $k_2^*\theta_{CH_2}$ together with reverse reactions are neglected.

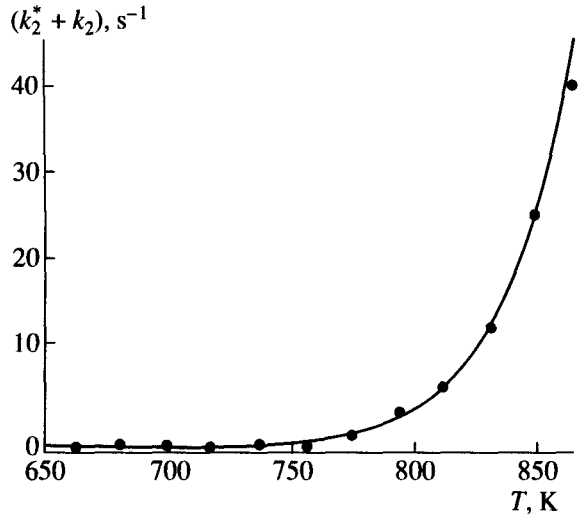

Fig. 10. A plot of the overall rate constant $k_2 + k_2^*$ for CH_2 decomposition versus temperature calculated by equation (30) (dots) and its approximation by the sum of two Arrhenius functions (curve).

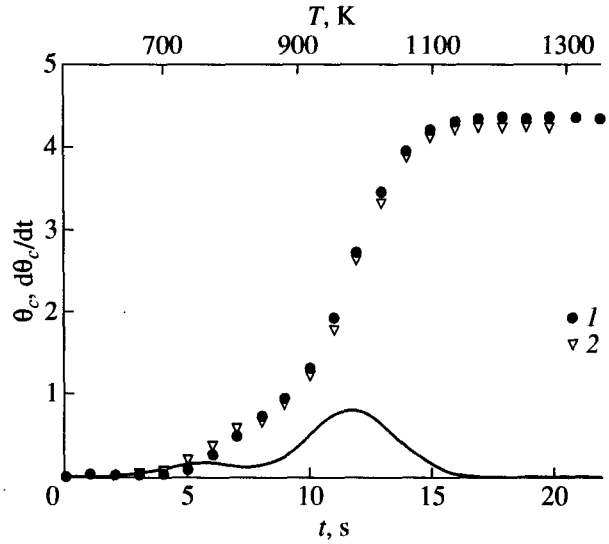

Fig. 11. Comparison of the curves of carbon accumulation calculated by (*1*) balance equation (22) and (*2*) rate law (26); (*3*) the rate of carbon formation calculated using the rate constants and surface coverages.

The apparent rate constant thus obtained is described by the Arrhenius equation (see Fig. 6):

$$k_{3\text{eff}} = 6 \times 10^{5 \pm 1} \exp((-90 \pm 5)/RT). \qquad (36)$$

Figure 11 compares the curves of carbon accumulation obtained from balance equation (22) and differential rate law (26) using the dependences of the rate constants k_2^* and $k_{3\text{eff}}$ and surface coverages θ_{CH_2} and θ_{CH} on time and temperature. As can be seen, these curves acceptably coincide with each other.

Analogously, we compared the $\theta_{CH}(t)$ dependence in the form of function (30) with that obtained by solving differential equation (25) while neglecting the reverse steps. Figure 7 illustrates the result of this comparison. In this case, the solution to equation (25) accurately describes the $\theta_{CH}(t)$ function at the initial period and in the vicinity of the maximum, whereas it gives the values lower than those obtained by equation (30) at the tail of the curve. This is likely due to the choice of approximating function (29), which rapidly decreases as moving farther from the maximum, and this results in the underestimated rates of CH formation. However, for the calculations of this sort, the agreement of the results may generally be acceptable.

The only detail that is not described by scheme (II) is that noticeable hydrogen desorption begins 3 s after methane desorption (at a 110 K higher temperature) (see Fig. 4). In connection with this, for $t < 3$ s, we obtained from equation (10) that $\theta_H = 0$ (Fig. 5). Therefore, the rate of methane formation by reaction 6 from scheme (II) should also be equal to zero. A trivial explanation is that we failed to determine hydrogen desorption at the initial stages because of a low sensitivity of the mass spectrometer. Therefore, in fact, $\theta_H > 0$ and $W_{CH_4} > 0$ in this region. Another possibility is the formation of methane without the participation of adsorbed hydrogen via the metathesis reaction

$$2[CH_3] \longrightarrow [CH_2] + CH_4.$$

Let us consider the rate constants obtained by analyzing scheme (II). They are compiled into the table and shown in the form of functions of temperature (Fig. 6).

Note that all rate constant are described well by the Arrhenius equation.

Interestingly, the rate constants of hydrogen atom recombination with each other k_5 and with CH_2 groups (k_{-1}) coincide over a broad range of temperatures (Fig. 6). This can be explained by the fact that the rates of these processes are limited by adsorbed hydrogen mobility.

On the other hand, the rate constant k_6 of hydrogen recombination with adsorbed CH_3 groups in the same temperature range is 20–30 times lower than k_5 and k_{-1}. This process is probably limited by the act of recombination itself, which is associated with steric hindrances. This is reflected in a lowered value of the preexponential factor of the rate constant k_6.

A lowered value of the preexponential factor of the apparent rate constant $k_{3\text{eff}}$ that describes the decomposition of surface CH groups into carbon and hydrogen is probably associated with the fact that this reaction is not elementary, because the reverse process and the diffusion of carbon into the metal bulk mentioned above may occur simultaneously.

For instance, if we consider that the concentration of surface carbon is pseudo-steady-state, $k_{3\text{eff}}$ can be

Parameters of rate constants according to scheme (II)

Reaction	k_i	k^0, s^{-1}	E, kJ/mol	T, K
$[CH_3] \longrightarrow [CH_2] + [H]$	k_1	$1.1 \times 10^{7 \pm 1}$	115 ± 4	550–670
$[CH_2] + [H] \longrightarrow [CH_3]$	k_{-1}	$1.1 \times 10^{13 \pm 1}$	151 ± 4	660–900
$[CH_2] \longrightarrow [CH] + [H]$	k_2	$2.0 \times 10^{14 \pm 1}$	210 ± 10	740–860
$[CH_2] \longrightarrow [C] + 2[H]$	k_2^*	0.7 ± 0.3	0 ± 5	660–760
$[CH] \longrightarrow [C] + [H]$	$k_{3\text{eff}}$	$6.0 \times 10^{5 \pm 1}$	90 ± 5	900–1100
$2[N] \longrightarrow N_2$	k_4	$3.0 \times 10^{13 \pm 1.5}$	280 ± 15	1000–1300
$2[H] \longrightarrow H_2$	k_5	$4.0 \times 10^{13 \pm 2}$	160 ± 10	750–950
$[CH_3] + [H] \longrightarrow CH_4$	k_6	$1.3 \times 10^{9 \pm 1}$	117 ± 6	700–830

described in the explicit form:

$$k_{3\text{eff}} = k_3 k_7 / (k_7 + k_{-3}\theta_H). \quad (37)$$

A change in the terms in the numerator of equation (37) with an increase in temperature probably leads to an underestimated value of the apparent preexponential factor.

Based on the analysis of experimental data, we conclude that CH_2 groups may directly decompose into carbon without CH formation.

Methyl groups adsorbed on the molybdenum surface and the products of methyl group decomposition (CH_2 and CH) are stable at temperatures below 600 K. Methylene groups are less stable and may decompose into CH and H or directly into carbon. They also can recombine with hydrogen atoms on the surface to form methyl groups.

ACKNOWLEDGMENTS

This work was supported by the International Science Foundation (grant nos. MBN300 and MN2000/2300) and the Russian Foundation of Basic Research (grant no. 95-03-08114).

REFERENCES

1. Driscoll, D.J., Campbell, K.D., and Lunsford, J.H., *Adv. Catal.*, 1987, vol. 35, p. 139.
2. Garibyan, T.A. and Margolis, L.Ya., *Catal. Rev.–Sci. Eng.*, 1989–1990, vol. 31, p. 35.
3. Sinev, M.Yu., Margolis, L.Ya., and Korchak, V.N., *Usp. Khim.*, 1995, vol. 64, no. 4, p. 373.
4. Nersessyan, L.A., Vardanyan, I.A., Kegeyan, E.M., *et al.*, *Dokl. Akad. Nauk SSSR*, 1975, vol. 220, no. 3, p. 605.
5. Driscoll, D.J., Martir, W., Wang, J.-X., and Lunsford, J.H., *J. Am. Chem. Soc.*, 1985, vol. 107, no. 6, p. 5062.
6. Tulenin, Yu.P., Sinev, M.Yu., Savkin, V.V., and Korchak, V.N., *Stud. Surf. Sci. Catal.*, 1997, vol. 110, p. 757.
7. Fairbrother, D.H., Peng, X.-D., Stair, P.C., *et al.*, *Proc. of the Symp. on Methane and Alkane Conversion Chemistry, 207th ACS National Meeting*, San Diego: CA, 1994, p. 280.
8. Hall, R.B., Castro, M., Kim, C.-M., *et al.*, *Proc. of the Symp. on Methane and Alkane Conversion Chemistry, 207th ACS National Meeting*, San Diego: CA, 1994, p. 282.
9. Yang, Q.Y. and Ceyer, S.T., *J. Vac. Sci. Technol. A*, 1988, vol. 6, no. 3, p. 851.
10. Smudde, G.H., Jr., Min, Yu., and Stair, P.C., *J. Am. Chem. Soc.*, 1993, vol. 115, no. 5, p. 1988.
11. Jentz, D., Trenary, M., Peng, X.D., and Stair, P., *Surf. Sci.*, 1995, vol. 341, no. 3, p. 282.
12. Bol, C.W.J., Kovacs, J.D., Chen, M., and Friend, C.M., *J. Phys. Chem. B*, 1997, vol. 101, no. 10, p. 6436.
13. Kislyuk, M.U. and Rozanov, V.V., *Kinet. Katal.*, 1995, vol. 36, no. 1, p. 89.
14. Kislyuk, M.U., Sklyarov, A.V., and Dangyan, T.M., *Izv. Akad. Nauk SSSR, Ser. Khim.*, 1975, no. 10, p. 2161.
15. Cerny, S., Ponec, V., and Hladek, L., *J. Catal.*, 1966, vol. 5, no. 1, p. 27.
16. Mahning, M. and Schmidt, L.D., *Z. Phys. Chem.*, 1971, vol. 75, p. 227.
17. Lapyonlade, J. and Neil, K.S., *C. R. Acad. Sci., Ser. C*, 1972, vol. 274, no. 4, p. 2125.
18. Ko, S.M. and Schmidt, L.D., *Surf. Sci.*, 1974, vol. 42, no. 3, p. 508.
19. Dushman, S., *Scientific Foundations of Vacuum Technique*, Lafferty, J.M., Ed., New York: Wiley, 1962, p. 715.
20. Trendelenburg, E.A., *Ultrahochvakuum*, Karlsruhe: G. Braun Verlag, 1963, p. 286.
21. King, D.A., *Chemistry and Physics of Solid Surfaces*, Wanselow, R. and Tong, S.Y., Eds., Boca Raton, FL: CRC, 1979, vol. 2, p. 87.